

STUDY ON ACOUSTIC PROPERTY OF HIGH POROSITY OPEN-CELL FOAMS BY HOMOGENIZATION APPROACH

Trinh Van Hai*

Le Quy Don Technical University

Abstract

This paper demonstrates a homogenization approach to characterize the effect of cell size of open-cell foam materials on their acoustic properties such as effective density, effective bulk modulus, and sound absorption. The three-dimensional representative volume element of the local morphology of open-cell foams is first reconstructed. The homogenization technique is then employed to calculate the effective acoustic properties of the foam materials. After a validation step, the proposed numerical framework is finally adapted to investigate the cell size-induced effect on the acoustic properties of foam-based absorbers. The obtained results indicate that, for a given high porosity, the tuned cell size can bring the desired effective and sound-absorbing properties. For two considered layers, the averaging cell size in the range of 0.15-0.45 mm shows better acoustic performance with an absorption ability > 80 %.

Keywords: Cellular material; cell size; permeability; tortuosity; effective and absorption property.

1. Introduction

Sound absorbing porous materials are composed of a matrix based on solid skeleton and a pore space (e.g., cavities, channels or interstices) which allows the sound waves propagating these media. Due to the combination of dissipation mechanisms when the air propagates within a porous medium, its freely propagating sound energy is absorbed. The acoustic performance of absorbing materials is governed by the mechanisms of acoustic energy dissipation during wave propagation in these media (see Fig. 1a for a diagram of an acoustic absorber excited by an acoustic wave). It is seen from numerous studies about acoustic problems that the acoustical behaviour (transport and absorptive properties) of absorbing layers is highly dependent on their local morphological parameters such as the porosity and the pore connectivity [1-3]. Thus, different approaches have been introduced in the literature to characterize analytically, numerically, and experimentally the correlation between the material local geometry and its macroscopic performance [4-7].

* Email: hai.tv@lqdtu.edu.vn

resemble isotropic high performance structural foams with relatively homogeneous cell geometries (see demonstrated examples shown in Fig. 2c-d). In this work, we focus on modeling porous media made from random close packing of mono-sized rigid spheres. In order to generate the sphere packings, the dynamically packed algorithm referred to molecular dynamics is used. This method is first introduced in Ref. [9] as follows. In this study, the initial state is N randomly distributed points that represent the center of spheres generated in a basic cube with a size of L . Each point is surrounded by two spheres: inner and outer ones. The outer diameter $d_{\text{out}}^{(0)}$ is set initially to $2L [3/(4\pi N)]^{1/3}$ corresponding to a nominal packing fraction of $\phi_p = 1$. The inner diameter $d_{\text{in}}^{(k)}$ is set to the minimum center-to-center distance between any two spheres after iteration k ,

$$d_{\text{in}}^{(k)} = \min \|\mathbf{r}_{ij}^{(k)}\| := \mathbf{x}_i^{(k)} - \mathbf{x}_j^{(k)}, \quad i, j \in [1, N] \text{ and } i \neq j \quad (1)$$

Initially, the inner diameter $d_{\text{in}}^{(0)}$ defines a true volume fraction which is very low, and the outer spheres do overlap each other. The algorithm then eliminates overlaps and slowly reduces the outer diameter. The inner and the outer diameters approach each other and the algorithm is halted by an eventual coincidence of the true and nominal packing fractions. In each step, the worst overlap between spheres i and j is eliminated by moving them apart an equal distance along the line joining their centers as

$$\begin{cases} \mathbf{x}_i^{(k+1)} = \mathbf{x}_i^{(k)} + D^{(k)} \mathbf{r}_{ij}^{(k)} \\ \mathbf{x}_j^{(k+1)} = \mathbf{x}_j^{(k)} + D^{(k)} \mathbf{r}_{ji}^{(k)} \end{cases}, \quad \text{with } D^{(k)} = \frac{1}{2} \frac{d_{\text{out}}^{(k+1)} - \|\mathbf{r}_{ij}^{(k)}\|}{\|\mathbf{r}_{ij}^{(k)}\|} \quad (2)$$

If any overlaps remain, reducing the outer diameter by the following equation,

$$\lambda^{(k+1)} = \lambda^{(k)} - \kappa_i / (2^\Gamma N) \quad (3)$$

in which $\lambda^{(k)} = d_{\text{out}}^{(k)} / d_{\text{out}}^{(0)}$ and $\Gamma = \lfloor -10 \log_{10} \Delta \phi_p^{(k)} \rfloor$. Parameter κ_i characterizing the initial rate of contraction of the ensemble is the initial contraction rate, which is independent of the size and number of spheres. $\Delta \phi_p^{(k)}$ is the difference between the nominal and true packing fractions at the iteration k , and symbol $\lfloor \cdot \rfloor$ is the greatest integer function.

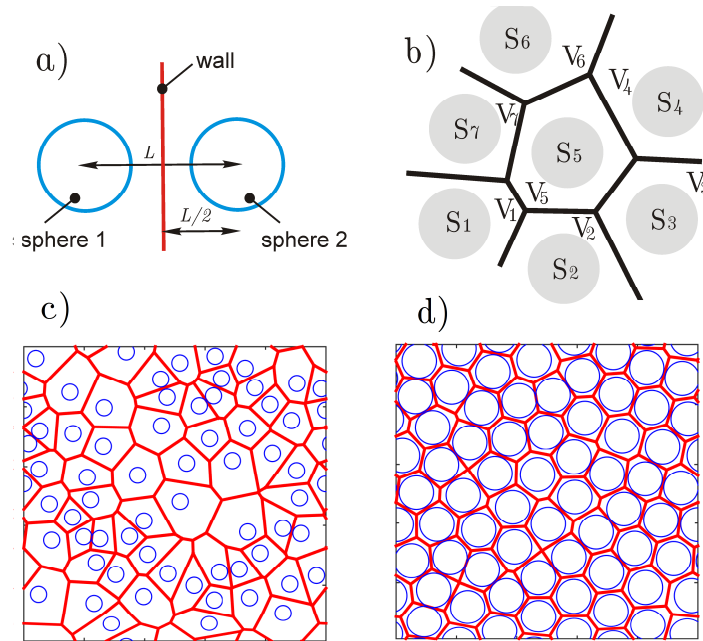


Fig. 2. Schematic illustration of Voronoi tessellation.

Top: wall generation between two neighborhood spheres (a) and two-dimensional demonstration of Voronoi process (b). Bottom: Voronoi diagrams for packing of equal-size hard circles with a fraction of 0.1 (c) and 0.7 (d), respectively.

In a Voronoi pattern, the partitioning is based on a set of seed points distributed in a model space where each cell is defined by all points that are closer to one particular seed point than to any others. Mathematically, given a set S of N points in a three-dimensional space, the process of associating all the locations of the space into polyhedral regions with the closest point of S is called Voronoi partitioning process. The polyhedral regions are called cells. The union of all the cells is then referred to as a Voronoi diagram. Theoretically, a Voronoi diagram may be constructed in any dimensional space. A cellular foam model based on Voronoi partitions of 3D space is built as follows:

First, a set of N nuclei (seed points) is given in a three-dimensional finite space R^3 . For each nucleus, let cell V_i be the region consisting of all locations in the space which are closer to P_i than any other nucleus P_j (with $j \neq i$). A cell V_L corresponding to seed point P_i is defined as:

$$V_L(\mathbf{x}_i) = \left\{ \mathbf{x} \in R^3 \mid \|\mathbf{x} - \mathbf{x}_i\| \leq \|\mathbf{x} - \mathbf{x}_j\| \quad \forall i \neq j \right\} \quad (4)$$

where \mathbf{x}_i and \mathbf{x}_j are the coordinates of seed points P_i and P_j , respectively.

Then, each seed point is surrounded by a cell containing all points in space that are closer to this particular seed point than to any other. Consequently, cell walls will appear centrally aligned on, and perpendicular to, lines that fictively connect two neighbor seed points. Cell edges appear wherever cell walls intersect and cell vertices appear where cell edges intersect (see Fig. 2b). The result is strictly convex cells with flat faces. An ordered set of seed points can be used for creating ordered and regular structures, for instance, structures made of Kelvin or Weaire-Phelan pattern. Voronoi algorithm generates around each seed a convex polyhedral unit cell made of vertices, joined by edges delimiting planar faces, which connect neighbor cells. Finally, a foam skeleton is completely established (see Fig. 3).

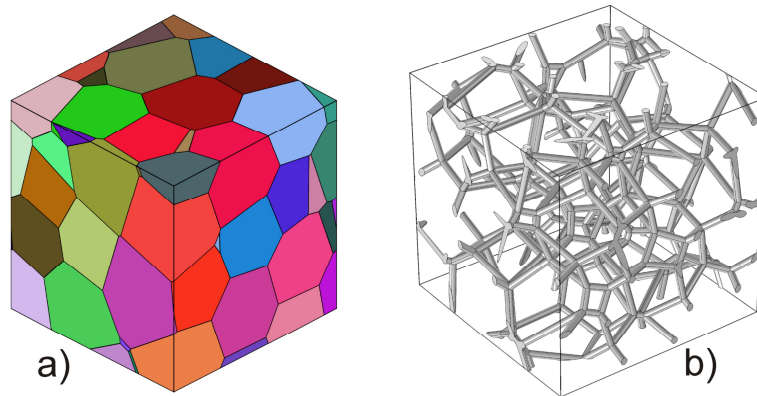


Fig. 3. Periodic Voronoi cell pattern (a) and the corresponding REV of cellular foams (b).

From the REV configuration Ω (within fluid phase Ω_f and solid-fluid interface $\partial\Omega$), the purely geometrical factors of porous cellular structure (e.g., the porosity ϕ and the thermal characteristic length Λ' also named the hydraulic radius) can be found as,

$$\phi = \frac{\iiint_{\Omega_f} dV}{\iiint_{\Omega} dV}, \quad \Lambda' = 2 \frac{\iiint_{\Omega} dV}{\iint_{\partial\Omega} dS} \quad (5)$$

3. Computations of transport and acoustic properties

In this section, we introduce briefly the first principles for computation of four transport properties. First, the low Reynolds number flow of an incompressible Newtonian fluid is governed by the usual Stokes equations in the fluid phase Ω_f :

$$\eta \Delta \mathbf{v} - \nabla p = -G, \quad \text{with } \Delta \cdot \mathbf{v} = 0 \quad (6)$$

where \mathbf{v} , p , and η are respectively the velocity, pressure, and viscosity of the fluid.

In general, \mathbf{v} satisfies the no-slip condition ($\mathbf{v} = 0$) at the fluid-solid interface. $G = \nabla p^m$ is a macroscopic pressure gradient acting as a source term. The static (viscous) permeability k_0 was obtained by averaging the velocity components in the fluid domains, Ω_f . The constant k_0 is often referred as the static thermal permeability. It can be shown that the non-vanishing components \mathbf{v}_x of the local velocity field are given by $\mathbf{v}_x = -\mathbf{k}_{0xx}G_x/\eta$. Here, \mathbf{k}_{0xx} is a scaled velocity field. Thus, the static viscous permeability k_{0xx} is calculated as:

$$k_0 = k_{0xx} = \phi \langle \mathbf{k}_{0xx} \rangle \tag{7}$$

where the symbol $\langle \cdot \rangle$ indicates a spatial average over the fluid-phase.

Secondly, in the high frequency limit, the viscous boundary layer becomes negligible and the fluid tends to act as a perfect one, having no viscosity except in the vicinity of the boundary layer. Consequently, the perfect incompressible fluid formally behaves as the potential flow problem:

$$\begin{cases} \nabla \cdot \mathbf{E} = 0, & \text{with } \mathbf{E} = -\nabla \varphi + \mathbf{e}, & \text{in } \Omega_f \\ \mathbf{E} \cdot \mathbf{n} = 0, & & \text{on } \partial\Omega \end{cases} \tag{8}$$

where \mathbf{e} is a constant unit vector, \mathbf{E} is the solution of the boundary problem having $-\nabla \varphi$ as a fluctuating part, and \mathbf{n} is the unit normal to the boundary of the pore region. The viscous characteristic length Λ and the high frequency tortuosity α_∞ are then calculated through,

$$\Lambda = 2 \frac{\iiint_{\Omega} |\mathbf{E}|^2 dV}{\iint_{\partial\Omega} |\mathbf{E}|^2 dS}, \quad \alpha_\infty = \frac{\langle |\mathbf{E}|^2 \rangle}{\langle |\mathbf{E}| \rangle^2} \tag{9}$$

Finally, the static thermal permeability k'_0 is estimated from the problem of thermal conduction as follows:

$$k'_0 = \langle \mathbf{u} \rangle \tag{10}$$

where the scaled temperature field u is solved from the canonical equations in fluid phase, $\Delta u = -1$, in which $u = 0$ on the solid-fluid interface.

In equivalent-fluid approach, an effective fluid is substituted for a porous medium with the effective density and effective bulk modulus. These effective factors are

introduced in the Johnson-Champoux-Allard-Lafarge (JCAL) model as,

$$\tilde{\rho}(\omega) = \rho_0 \phi \left[\alpha_\infty - j \frac{\eta \phi}{\omega \rho_0 k_0} \sqrt{1 + j \omega \frac{\rho_0}{\eta} \left(\frac{2k_0 \alpha_\infty}{\phi \Lambda} \right)^2} \right] \quad (11)$$

$$\tilde{K}(\omega) = \frac{\gamma P_0}{\phi} \left\{ \gamma - (\gamma - 1) \left[1 - j \frac{\phi \gamma P_0}{k'_0 C_p \rho_0 \omega} \sqrt{1 + j \frac{4k'_0{}^2 C_p \rho_0 \omega}{\gamma P_0 \Lambda'^2 \phi^2}} \right]^{-1} \right\}^{-1} \quad (12)$$

where ρ_0 is the air density, P_0 is the atmospheric pressure, $\gamma = C_p/C_v$ is the ratio of heat capacities at constant pressure and volume, j is the imaginary unit, η is the dynamic viscosity. Six parameters (ϕ , Λ' , k_0 , α_∞ , Λ , and k'_0) are the geometric and transport properties mentioned previously.

The sound absorption coefficient at normal incidence SAC_{NI} of this homogeneous layer is derived as the following equation:

$$SAC_{NI} = 1 - \left| \frac{\tilde{Z}_s(\omega) - Z_0}{\tilde{Z}_s(\omega) + Z_0} \right|^2 \quad (13)$$

where Z_0 is the characteristic impedance of the air and $\tilde{Z}_s(\omega)$ is the normal incidence surface impedance of the layer, having a thickness of H_s . This surface acoustic impedance is estimated as,

$$\tilde{Z}_s(\omega) = -j \sqrt{\tilde{\rho}(\omega) \tilde{K}(\omega)} \cot \frac{\omega H_s}{\sqrt{\tilde{\rho}(\omega) / \tilde{K}(\omega)}} \quad (14)$$

4. Results and discussion

Following above-described framework, we solve flow and thermal problems over the RVE with the symmetry condition on its lateral surfaces by COMSOL Multiphysics[®] v5.2. In its modules, we implement the corresponding governing equations in the REV Ω with a fluid domain Ω_f and a fluid-solid interface $\partial\Omega$ (see Fig. 3b for the solid phase of the RVE).

Before investigating the acoustical behavior of foam materials, the proposed method is first validated by a reference example. The work by Gasser et al. [7] is one of the first works where the sound absorption of rigid porous media (made up of identical rigid spheres) is calculated from micro-structure using the finite element method. The regular face centered cubic (FCC) packing of rigid spheres was assumed with a porosity

of 0.26 with the radius of the spheres was 1 mm (noted that this ordered structure has a soldering neck of radius 150 μm binding the beads). Herein, as shown in Fig. 4 (some sub-figures are plotted with logarithmic scales), we first compare our numerical predictions of effective properties (dash line) of FCC structure with the reference data (circle markers) taken from Ref. [7].

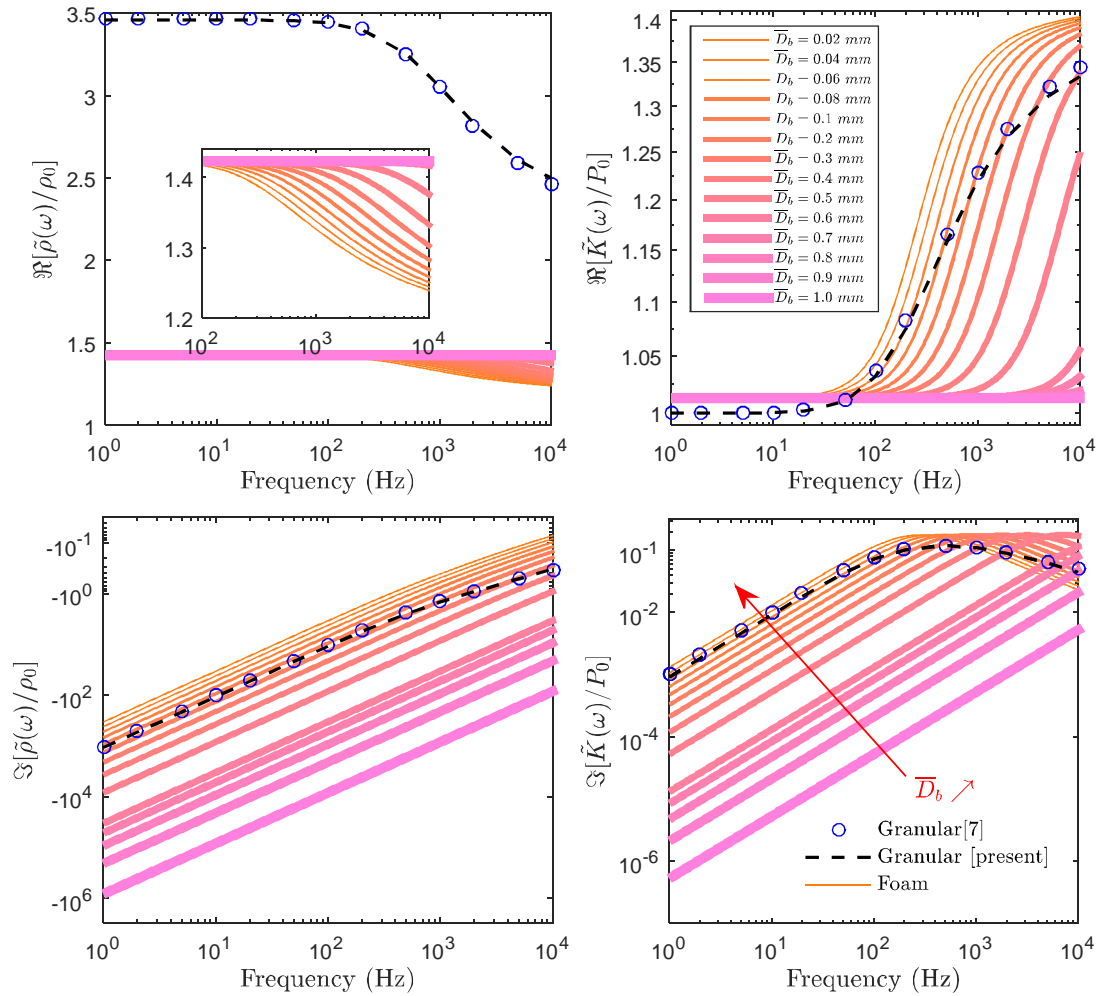


Fig. 4. The normalized effective density (left parts) and the normalized effective bulk modulus (right parts) of foams (continuous lines) in comparison with granular as FCC packing (markers for reference data and dash line for present work).

The effective density and bulk modulus of foam materials with an averaging cell size \bar{D}_b varying from 0.02 mm to 1 mm and a constant porosity ϕ of 0.98 were computed for a set of frequencies ranging from 1 Hz to 10⁴ Hz (see continuous lines in

Fig. 4, the thicker line is, the smaller cell size is). The obtained good agreement validates strongly our proposed numerical procedure.

From the obtained curves, we can state that: (i) the cell size affects strongly on two effective properties (both real and imaginary parts); (ii) the effective properties of the granular layer are different from those of foam connectivity. In term of material behaviors, we can see that the real part of granular effective density is far higher than the foamy one (the top left part of Fig. 4), whereas at the same scale the effective bulk modulus of both structures are quiet similar (remaining parts of Fig. 4). The effective behaviors of foams lead to their interesting sound absorption mentioned below.

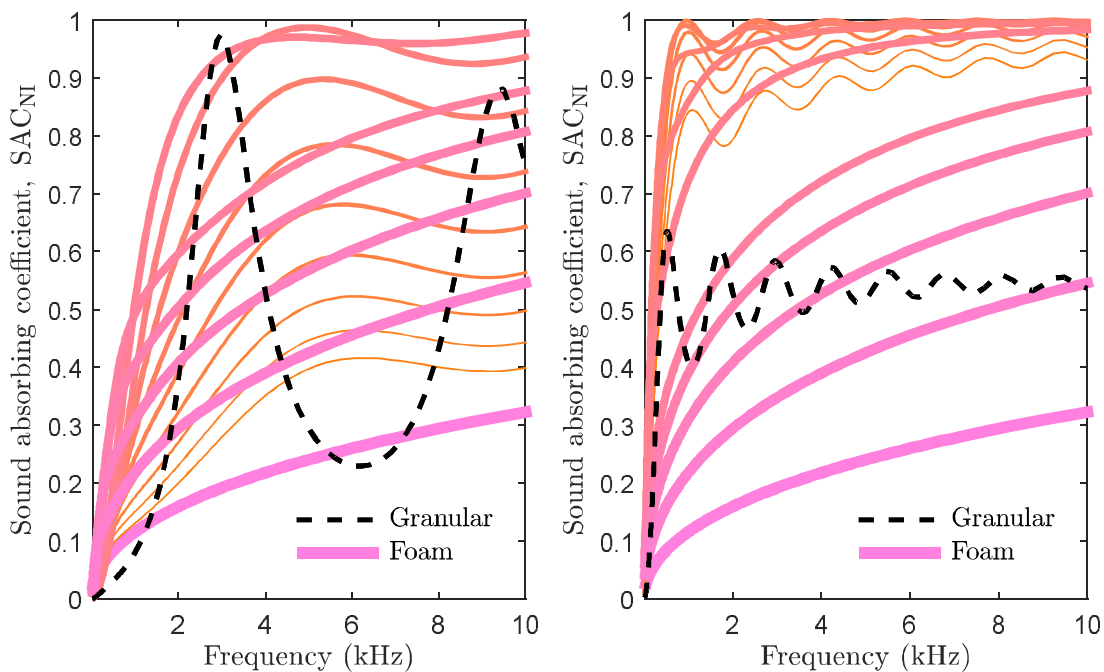


Fig. 5. Comparison of sound absorption coefficients of foam-based absorbers having a tuned cell size (continuous lines with legends as shown in Fig. 4) and a granular layer (dash lines).

Figure 5 plots the sound absorbing coefficient curves of open cell foam- and granular-based absorbers (left part for $H_s = 20$ mm, and right part for $H_s = 100$ mm). For investigated both thicknesses, the foam structures show a better performance of acoustic absorptions in comparison with the granular layer. In detail, for 20 mm-thick absorber, in order to obtain more than 80% of the incident sound energy at frequencies > 3 kHz, the averaging cell size should be selected in the range of 0.15-0.45 mm, whereas for 100 mm-thick absorber, the SAC can reach a level of 90% at low frequencies (i.e., 0.5 kHz) with the same value in

range 0.15-0.45 mm and for layers with a 80%-absorption ability at frequencies > 1 kHz, the averaging cell size range should be extended to a large range of 0.2-0.9 mm.

5. Conclusions

In this paper, we investigated the effective and absorption property of porous foam-based absorbers by a homogenization approach. The REV of foams has been generated based on the random close packing of rigid mono-sized spheres. Then, from the reconstructed REV, the geometric and transport properties were numerically calculated, and the effects of the cell size on the effective and absorption properties of foam structures have been studied. Generally, as the obtained SAC curves in the automobile frequency range, the derived SAC of a foam-based absorber can be obtained by tuning together its thickness and its local cell size. The sound absorption of high porosity open-cell foams can be improved at specific frequency ranges by either increasing the absorber thickness H_s or choosing a suitable cell size D_b .

Acknowledgements

This work is funded by Vietnam National Foundation for Science and Technology Development (NAFOSTED) under Grant Number 107.01-2019.316.

References

1. Delany, M.E. and E.N. Bazley (1970). Acoustical properties of fibrous absorbent materials. *Applied Acoustics*, 3(2), 105-116.
2. Doutres, O., N. Atalla, and K. Dong (2011). Effect of the microstructure closed pore content on the acoustic behavior of polyurethane foams. *Journal of Applied Physics*, 110(6), 064901.
3. Boutin, C. and C. Geindreau (2008). Estimates and bounds of dynamic permeability of granular media. *The Journal of the Acoustical Society of America*, 124(6), 3576-3593.
4. Trinh, V. H. (2018). *Effect of membrane content on the acoustical properties of three-dimensional monodisperse foams: Experimental, numerical and semi-analytical approaches*. Ph.D. Dissertation, Paris-Est University.
5. Perrot, C., F. Chevillotte, and R. Panneton (2008). Bottom-up approach for microstructure optimization of sound absorbing materials. *The Journal of the Acoustical Society of America*, 124(2), 940-948.
6. J. F. Allard and N. Atalla (2009). *Propagation of sound in porous media: Modelling sound absorbing materials* (2nd Edition). John Wiley & Sons.
7. Gasser, S., F. Paun, and Y. Bréchet (2005). Absorptive properties of rigid porous media: Application to face centered cubic sphere packing. *The Journal of the Acoustical Society of America*, 117(4), 2090-2099.

8. Doutres, O., N. Atalla, and K. Dong (2013). A semi-phenomenological model to predict the acoustic behavior of fully and partially reticulated polyurethane foams. *Journal of Applied Physics*, 113(5), 054901.
9. Gao, K., J. van Dommelen, and M. Geers (2016). Microstructure characterization and homogenization of acoustic polyurethane foams: Measurements and simulations. *International Journal of Solids and Structures*.
10. Hoang, M.T. and C. Perrot (2012). Solid films and transports in cellular foams. *Journal of Applied Physics*, 112(5), 054911.
11. Hoang, M.T., et al. (2014). Linear elastic properties derivation from microstructures representative of transport parameters. *The Journal of the Acoustical Society of America*, 135(6), 3172-3185.
12. Langlois, V., et al. (2018). Permeability of solid foam: Effect of pore connections. *Physical Review E*, 97(5), 053111.
13. Viet Dung, V., R. Panneton, and R. Gagné (2019). Prediction of effective properties and sound absorption of random close packings of monodisperse spherical particles: Multiscale approach. *The Journal of the Acoustical Society of America*, 145(6), 3606-3624.

NGHIÊN CỨU ĐẶC TÍNH ÂM CỦA CẤU TRÚC XÓP MỎ CÓ ĐỘ RỖNG CAO BẰNG PHƯƠNG PHÁP ĐỒNG NHẤT HÓA

Tóm tắt: Bài báo trình bày phương pháp đồng nhất hóa để nghiên cứu sự ảnh hưởng của kích cỡ tế bào vật liệu xốp mở đến các tính chất âm học như mật độ và mô đun khối hiệu dụng và khả năng hấp thụ âm thanh. Đầu tiên, phần tử khối đặc trưng ba chiều của hình thái cơ sở của cấu trúc xốp tế bào mở được xây dựng. Tiếp đến, kỹ thuật đồng nhất hóa được sử dụng để tính toán các đặc tính âm hiệu dụng của xốp. Cuối cùng, sau bước kiểm chứng, mô hình số đề xuất được sử dụng để khảo sát ảnh hưởng kích cỡ tế bào đối với các đặc tính âm của vật liệu xốp. Kết quả thu được chỉ ra rằng, ở độ rỗng cao nhất định việc điều chỉnh kích cỡ tế bào đem lại các đặc tính hiệu dụng và hấp thụ âm mong đợi. Đối với hai lớp hấp thụ đề cập, kích cỡ tế bào trung bình trong phạm vi 0,15-0,45 mm cho hiệu quả âm tốt với khả năng hấp thụ > 80%.

Từ khóa: Cấu trúc xốp; kích cỡ tế bào; độ thấm; độ xoáy; đặc tính hiệu dụng và hấp thụ.

Received: 12/3/2020; Revised: 20/7/2020; Accepted for publication: 28/7/2020

